Five-Core 1 × 6 Core Selective Switch and Its Application to Spatial Channel Networking

Masahiko Jinno, Takahiro Kodama, and Tsubasa Ishikawa
Department of Engineering and Design, Kagawa University, 2217-20 Hayashi-cho, Takamatsu 761-0396 Japan
jinno@eng.kagawa-u.ac.jp

Abstract: We design and prototype a 5-core 1 × 6 core selective switch (CSS) with an integrated input and output multi-core-fiber collimator and spatial multiplexer/demultiplexer array. Spatial bypassing and spectral grooming using a CSS-based hierarchical cross-connect are demonstrated.

1. Introduction

A spatial channel network (SCN) is a novel optical network architecture, which was proposed in 2018. In the SCN, the current optical layer is explicitly evolved into the hierarchical space division multiplexing (SDM) layer and wavelength division multiplexing (WDM) layer, and a conventional optical node is decoupled into a spatial channel cross-connect (SXC) and a wavelength cross-connect (WXC) to form a hierarchical optical cross-connect (HOXC) [1-6]. By doing so, future ultra-high capacity optical signals, which will have a bit-rate of 10 Tb/s and beyond [7], will be able to bypass the overlying WXCs in the WDM layer (*spatial bypass*) using potentially low cost and low insertion loss SXCs. This brings about significant reduction in the routing cost-per-bit in an optical transport network and considerable increase in the optical reach [1-4]. Here, a spatial channel (SCh) is defined as an ultra-high capacity optical data stream that is allowed to occupy the entire available spectrum of a spatial lane, whose physical entity is a core in a single mode fiber (SMF) or multi-core fiber (MCF).

As a growable and reliable SXC architecture in an SCN, our research group recently proposed a novel SXC architecture [1,2] based on a new type of optical spatial switch, which is referred to as a $1 \times n$ core selective switch (CSS), which is shown in Fig. 1(a). In order to pack optical (wavelength) channels (OChs) efficiently into an SCh, a conventional WXC is connected to add/drop ports of the SXC. Here, a CSS is the SDM counterpart of a conventional wavelength selective switch (WSS) in a current WDM network and incorporates functionalities for spatially demultiplexing SChs from a common SDM port and for switching and multiplexing any of them into any of n output SDM ports. Such functionality can be achieved by configuring functionalities of spatial demultipling, $1 \times n$ optical switching, and spatial multiplexing arranged as shown in Fig. 1(b),

A feasibility demonstration for a CSS employing discrete bulk optics comprising MCF fan-in fan-out (FIFO) devices and commercial 1 × 4 optical switches was recently conducted [6]. A preliminary switching experiment for a CSS based on free-space-optics was also performed using an input MCF collimator, an output MCF collimator mounted on a two-dimensionally movable stage to emulate multiple closely arranged output MCF collimators, and a liquid-crystal-on-silicon (LCoS) spatial light modulator (SLM) [5]. In this paper, we report for the first time a compact 5-core 1 × 6 CSS prototype, which has an integrated input and output multi-core fiber collimator and spatial multiplexer/demultiplexer array, and demonstrate its application to spatial channel networking, where 900-Gb/s spatial channels are spatially bypassed or spectrally groomed.

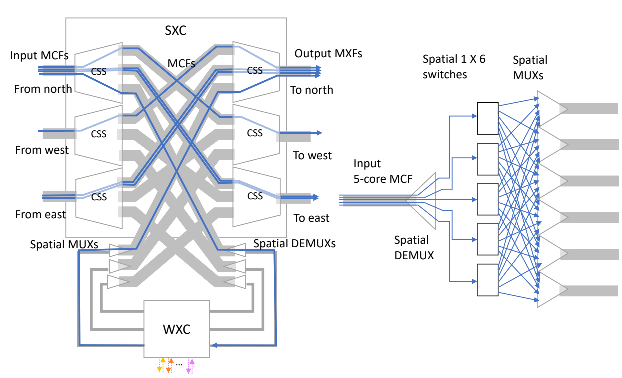

(a) Architecture of HOXC based on CSS (b) Equivalent circuit of CSS

Fig. 1. HOXC architecture based on CSS.

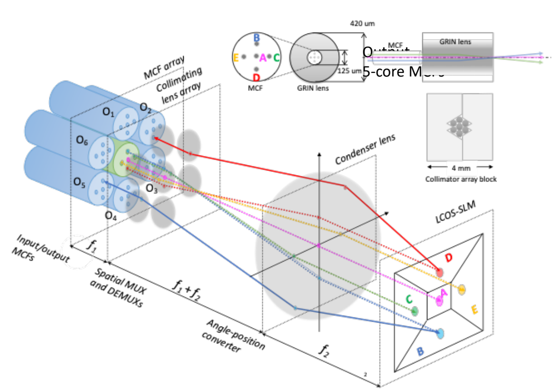

Fig. 2. Operating principle of 5-core 1 × 6 CSS prototype with integrated input/output MCF collimator array.

2. Configuration and Operating Principle of a Free-Space-Optics Based CSS Prototype

Figure 2 shows the configuration and operating principle of a free-space-optics based 5-core 1 × 6 CSS prototype. The basic operating principle of a CSS is the same as that described in [5]. A 5-core MCF, whose mode field diameter, core spacing, and cladding diameter are 9 µm, 44.8 µm, and 125 µm, respectively [8], was attached to a 0.25 pitch graded-index (GRIN) lens, whose effective focal length f_1, effective lens diameter, and outer diameter are 530 µm, 250 µm, and 420 µm, respectively, to achieve an MCF collimator. Seven MCF collimators are arranged in the hexagon close-packed structure with the same rotational core arrangement to achieve an integrated input and output MCF array. Here, each MCF and each core in the MCFs is indexed as shown in the inset to Fig. 2 using labels of input MCF I0 (center MCF), output MCF O_1-O_6 (outer MCFs), and core A (center core), and cores B-E, (outer cores). Five beams from five cores of the input MCF converge to the same spot at the end of the GRIN lens. Since the center core position coincides with the optical axis of the lens, the beam from the central core goes straight along with the optical axis of the lens, while the beam from an outer core is launched with polar and azimuthal angles corresponding to the position of the core in the cross section of the MCF. This means that the collimating lens attached to the MCF acts as a spatial multiplexer and demultiplexer. A condenser lens (f_2 = 50 mm) is set to form a tele-centric configuration with the collimator lenses. Five beams from each core of the input MCF focus on different positions at an LCoS-SLM according to their emitting angle at the end of the GRIN lens. Due to the tele-centric configuration, the five spots on the LCoS-SLM represent a point-symmetric expanded image of beams at the input MCF with magnification factor M of f_2/f_1.

The LCoS-SLM was partitioned into five areas. By changing the period and direction of the 2π saw-tooth hologram in each area, each beam from the input MCF is steered independently to a core with the same index in its designated output MCF (core-by-core switching). Because in practical SXC applications there is most likely no need to change seamlessly the switching area, which is required for flexible-grid-enabled WSSs, two-dimensionally arrayed micro-electro-mechanical-system (MEMS) mirrors that excel in terms of larger switching angles and polarization independency can also be used as a switching element. In this demonstration, we employed an LCoS-SLM because of its advantageous software-configurability feature, which is useful especially in experiments, although it necessitates additional polarization diversity optics (not shown in Fig. 2 for better visibility).

Figure 3 shows images of the 5-core 1×6 CSS prototype employing an LCoS-SLM (Santec Corporation SLM-100). Since an integrated GRIN lens array serves both as collimator lenses and spatial multiplexer/demultiplexers, the CSS prototype is very compact in the order of double the focal length of the condenser lens (50 mm) and the size of the LCoS (10 mm × 15 mm). Roughly speaking in CSS design, the achievable port count and/or number of supportable cores per fiber increase in proportion to the square of the maximum steering angle θ_{max} of the switching element and the device length decreases in proportion to θ_{max}. A larger scale or smaller size CSS may be achieved by employing a two-dimensional MEMS array.

3. CSS Performance Evaluation and Spatial Channel Networking Demonstration

Figure 4 shows the average insertion loss (IL) and the polarization dependent loss (PDL) at 1550 nm including the excess loss of two FIFO devices used for the IL measurement (0.9 dB ~ 1.4 dB) and the LCoS diffraction loss (~ 1 dB) when cores A~E of the input MCF are connected to output MCFs O_1~O_6. Output MCFs O_1, O_4, and O_5 show relatively high IL and/or PDL probably due to the imperfection of the GRIN-MCF alignment. The minimum IL of 4.0 dB and PDL of 0.7 dB are achieved for Core-C of output MCF O_2. No wavelength-dependent loss was observed over

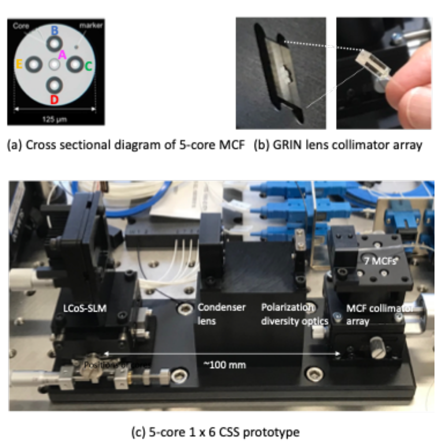

Fig. 3. Images of 5-core 1 × 6 CSS prototype.

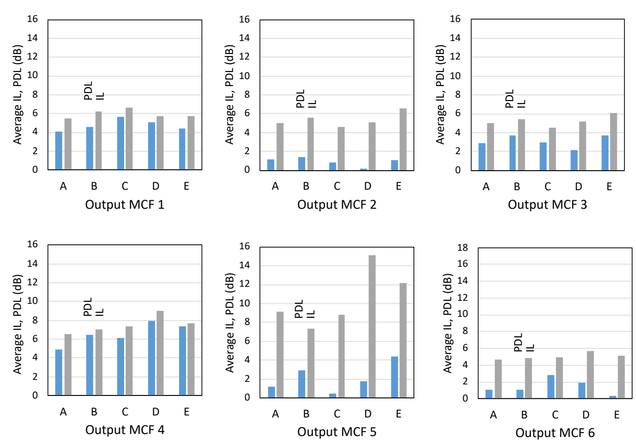

Fig. 4. Average IL and PDL of 5-core 1×6 CSS prototype.

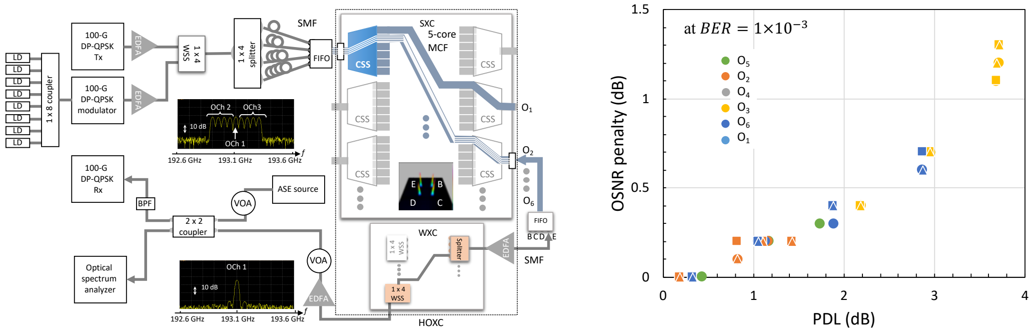

(a) Experimental configuration for BER performance measurement in core selective switching using 5-core 1 x 6 CSS prototype

(b) OSNR penalty plotted as a function of PDL for each connection

Fig. 5. BER performance measurement for spatially bypassed or spectrally groomed spatial channels using a CSS-based HOXC. Circles, squares, triangles in Fig. 5(b) indicate the OSNR penalty under the conditions (A), (B), and (C), respectively.

the C-band. These observations indicate that the free-space-optics based CSS architecture will potentially provide low net IL at the level of ~ 2 dB for all output MCFs if the non-uniformity of the IL in MCF collimators is improved as the manufacturing technology matures and a two-dimensional MEMS mirror array is employed instead of an LCoS-SLM. We measured inter-core crosstalk (XT) when all cores are connected to the same output MCF. Most cores indicate high inter-core XT exceeding 40 dB. Relatively low inter-core XT from an outer core to a diagonal outer core at the level of ~32 dB was observed, which is considered to be caused by higher-order diffraction from the LCoS.

Using the experimental configuration shown in Fig. 5(a), we tested the CSS prototype implemented in an HOXC by measuring the pre-forward error correction bit error rate (pre-FEC-BER) under the conditions below.

(A) A single 100-Gb/s DP-QPSK signal is switched by the CSS to output MCFs O_1~O_6.

(B) Four 100-Gb/s DP-QPSK signals with the same center frequency that are spatially multiplexed, each propagating in a different outer core of an MCF, are switched by the CSS to the same output MCFs O_1~O_6.

(C) Four spectrally multiplexed single 100-Gb/s DP-QPSK signals and two 400-Gb/s DP-QPSK signals that are spatially multiplexed, each propagating in a different outer core of a 5-core MCF, are switched by the CSS to the same output MCFs O1~O6 and groomed by a WXC.

Figure 5(b) shows the OSNR penalty for 100-Gb/s DP-QPSK signals under each condition (A) ~ (C) as a function of the PDL that they experienced. We can see that the optical signal-to-noise ratio (OSNR) penalty only increases as the PDL increases. Neither the inter-core XT nor spectral grooming causes the increase in OSNR penalty. This indicates that we can expect a negligible OSNR penalty for all CSS connections if GRIN-MCF alignment is improved.

4. Conclusion

We demonstrated a compact 5-core 1×6 CSS having an integrated input and output MCF array with spatial multiplexer/demultiplexers for the first time. Performance evaluation of the CSS prototype including spatial bypassing and spectral grooming of a 900-Gb/s spatial channel indicates that the CSS enables a low-loss, distortion-free, and small foot-print SXC that will be needed in future SCNs in the forthcoming SDM abundant era.

Acknowledgements

The authors thank Furukawa Electric Co., Ltd. for their technical supports on MCFs and FIFO devices. This work was supported in part by the JSPS KAKENHI Grant Numbers 26220905/JP18H01443, and the National Institute of Information and Communication Technology (NICT) Grant Numbers 19302/20401.

References

[1] M. Jinno, "Spatial channel network (SCN): Opportunities and challenges of introducing spatial bypass toward massive SDM era [Invited]," J. Opt. Commun. Netw., vol. 11, no. 3, pp. 1-14, 2019.

[2] M. Jinno, "Spatial channel network (SCN) architecture employing growable and reliable spatial channel cross-connects toward massive SDM era," PSC 2018, Fr3C.5.

[3] M. Jinno, "Added value of introducing spatial bypass into WDM/SDM networks: Gaussian-noise model analysis for spatially-bypassed and spectrally-groomed optical channels," ECOC 2018, We3D.6.

[4] M. Jinno and Y. Asano, "Required link and node resource comparison in spatial channel networks (SCNs) employing modular spatial channel cross-connects (SXCs)," OFC 2019, M1A.1.

[5] M. Jinno, K. Yamashita, and Y. Asano, "Architecture and feasibility demonstration of core selective switch (CSS) for spatial channel network (SCN)," OECC/PSC 2019, WA2-3.

[6] M. Jinno, T. Kodama, T. Ishikawa, *et al.*, "Demonstration of spatial channel networking using two types of hierarchical optical cross-connects," ECOC 2019, Th.1.A.6.

[7] P. J Winzer and D. T Neilson, "From scaling disparities to integrated parallelism: A decathlon for a decade," J. Lightwave Technol., vol. 35, no. 5, pp. 1099-1115, 2017.

[8] T. Gonda, K. Imamura, M. Tsukamoto, et al., "Design of multicore fiber having upgradability from standard single-mode fibers and its application," J. Lightwave Technol., vol. 37, no. 2, pp. 396-403, 2019.